

# Simple-shear experiments on basement-cover sequences with a comparison to the Bierzo basin, NW Spain.

JEAN-CLAUDE SOULA, GILBERT BESSIÈRE & GERARD HERAIL

Soula, J.-C., Bessière, G., & Herail, G. 1988 12 30: Simple-shear experiments on basement-cover sequences with a comparison to the Bierzo basin, NW Spain. *Bulletin of the Geological Institutions of the University of Uppsala*, N.S., Vol. 14, pp. 163-179. Uppsala. ISSN 0302-2749.

Model experiments were carried out in order to analyse the behaviour of ductile, brittle or ductile-brittle basement with pre-existing faults beneath a sedimentary cover during deformation by finite simple shear.

Processes which have been studied in detail are the rotation of the fractures in different experimental materials; the sense of strike-slip motions and dip-slip motions along the faults; strain patterns along the faults; the opening and closing of the fractures as a function of their initial orientation; and the mechanisms responsible for the observed deformation.

In the basement, all faults rotated in the same sense as the bulk shear but the sense of finite strike-slip displacement is practically the same as the infinitesimal state. A shortening at the leading edge and an extension at the trailing edge on both sides of the faults accommodate the relative displacement and are responsible for uplifts facing depressed areas at fault ends and for dip-slip motions. Only the faults situated in the shortening field of the infinitesimal strain ellipsoid can open. Those in the extension field always close, even though the opening is essentially due to pull-apart parallel to the master-shear plane.

In the cover, basins only form along faults in the shortening field. The deformation in the basin over all basement faults is a combination of shortening and strike-slip simple shear parallel to the fault, dip-slip motion at fault tips and pull-apart parallel to the master shear plane. Pull-apart and push-up structures form only above basement faults at a low angle to the master shear plane where the simple shear component is dominant. Shortening parallel to the basement faults is dominant when these faults are at moderate angles (30 to 60°) to the master shear plane and is responsible for conjugate faults with acute bisectrices parallel to the basement fault and symmetrical structures in the cover.

Structures similar to those observed in natural basins are seen in the models, e.g. collapsed rhombohedral and triangular blocks, and lateral debris cones developing from intersecting conjugate faults arranged on both sides of a drainage axis.

Experimental results are compared to the Miocene Bierzo basin, NW Spain, which is interpreted as due to a regional left-lateral strike-slip shearing acting along NW-SE trending regional major faults responsible for the opening of pre-existing NE-SW and E-W faults with dextral antithetic strike-slip relative displacement along the NE-SW faults.

*J.-C. Soula & G. Bessière, Laboratoire de Géologie, Université Paul Sabatier, 38 rue des Treize-Six Ponts, 31400 TOULOUSE, France.*

*G. Herail, CIMA-UA 366 CNRS, Institut de Géographie D. Faucher, Université de Toulouse-Le Mirail, 5 allées A. Machado, 31058 TOULOUSE Cedex, France. Received 17th June 1987; revision received 19th February 1988.*

## Introduction

Scaled experimental models have long been used to investigate structural patterns in strike-slip zones. Early models analysed the behaviour of a brittle or ductile-brittle cover above a strike-slip fault and modelled fault patterns in strike-slip zones (e.g. Cloos 1928, Cloos 1955, Oertel 1965, Tchalenko 1970, Wilcox et al. 1973, Gamond & Giraud 1982, Deramond et al. 1983, Gamond 1985). The faults in these simple shear experiments developed as conjugate systems with acute bisectrices at 45° to the master shear plane, i.e. parallel to the major com-

pressive stress and to the axis of maximum compressive infinitesimal strain. The conjugate faults are well-known as Riedel shears. Even though not always explicitly quoted by the authors, the experimental alternation of pull-aparts and push-ups would be capable of controlling the sedimentation in natural basins. Recently, model experiments were done by Whithjack & Jamison (1986) to investigate the effects of oblique extension, i.e. strike-slip shearing with an extensional component (combination of simultaneous simple shear and pure shear in the sense of Ramberg 1975a, b). However, these model experiments are focused on fault pat-

terns in oblique rifting but not on the tectonic control of sedimentation.

Recent studies associating sedimentological and structural field studies have improved our knowledge of the tectonic control of sedimentation, especially in detrital deposits (e.g. control of the origin of debris cones by intersecting faults, sedimentation controlled by tilted blocks at high angles to the master fault, location of depocentres in pull-apart structures, development of rhombohedral basins). Some sedimentologists working in areas where a strike-slip system is suspected have used previous experimental models as a key to interpret their sedimentological data (e.g. Garfunkel et al. 1981, Cabrera et al. 1988, Debroas 1987, Larouzière et al. 1987, Montenat et al. 1987). However, strict application of the models has been restricted to simple situations such as basins developed at the ends of single strike-slip faults or relays of en échelon faults. Concurrently other sedimentologists have proposed conceptual tectonic models involving a tectonic control of sedimentation from their observations of natural sedimentary structures but without the support of experimental or theoretical mechanical models (e.g. Crowell 1974 or Steel & Gloppen 1980). However some of the mechanisms proposed by these authors, such as the development of normal faults at much more than 90° to the shear plane in simple shear, seem at first sight contradictory to the previous experimental models and need to be tested. In any event, empirical rules for the diagnosis of sedimentation related to strike-slip shearing have been deduced from these sedimentological – structural studies.

The fundamental goal of the present study is to investigate the development and evolution of basins related to the activity of several preexisting faults with differing orientations capable of interfering. Experiments will also be used to test previous conceptual models. The experimental approach has been chosen because theoretical or numerical approaches to this problem are still complex. One of the long-term goals of this study is to use the results as a basis for theoretical studies. Another advantage is that some large-scale sedimentary structures can be duplicated (Soula et al. 1979).

The study is focused on inter-mountain basins because numerous tectonic and sedimentological data are now available for these basins and because their limited dimensions allow a detailed analysis of the individual troughs in a composite basin. The structures in the basement are often rather well-known and it is possible to observe their activity within the basin. In addition, the effects of thermal phenomena or of large-scale subsidence have no noticeable consequence.

## Experimental models of strike-slip deformation

### *Methods*

The shear box used in the present experiments is composed of two sliding rigid half-plates with an L section and is similar to the apparatus used by previous workers (e.g. Tchalenko 1970, Wilcox et al. 1973, Gamond et Giraud 1982, Soula 1984, amongst others). Because of the complexity of the problem, the experiments were done in simple shear.

As in most of the previous experiments, tests have been carried out in order to analyse the behaviour of a brittle or a ductile-brittle cover above a strike-slip master fault in a rigid basement. However, because of the fundamental goal of this study, ductile basement with or without discontinuities was also used. Even though it seems obvious that the actual "basement" of the basins, i.e. the uppermost crust, had a ductile-brittle behaviour, a ductile layer has been used because ductile syn-sedimentary deformation is effectively observed in many rock types and marked by e.g. synsedimentary folds or roll-overs. Moreover, the basement rocks are not necessarily very brittle (e.g. marls, schists) and may deform by continuous deformation or by slip along discrete but penetrative discontinuities (pre-existing cleavages, foliations or mesoscopic faults). These preexisting penetrative discontinuities might have acted together and the von Mises ductility criterion which requires 5 independent slip systems for the rock to have a ductile behaviour was probably satisfied. In addition, because the faults have finite lengths, ductile deformation is necessary at their ends for displacement along them to occur. On more general grounds, little is known concerning the possible consequences in the cover of ductile deformation of basement. In any event, the exaggeration arising from the use of ductile material makes easier a detailed qualitative analysis of the deformation.

### *Model materials.*

Plasticine has been frequently used for simulating rock behaviour (e.g. Ramberg 1982, Dixon & Summers 1985). Its properties and its suitability as a scaled analog for rocks have been analysed in detail by McClay (1976) and Dixon & Summers (1985). McClay (1976) found a power law flow behaviour with a stress exponent within the range  $n = 6-9$ . However, Dixon and Summers (1985) found that a simple extrapolation of McClay's results to high strain rates, i.e.  $10^{-2} \text{ s}^{-1}$  and faster, is not valid and they proposed a readjusted curve based on experi-

mental analyses of enbankment slopes carried out by Stevens (1983). The plasticine we used in our models was tested in a shear box for soil mechanics and displayed a cohesion of 50–60 kPa at 18°C at strain rates of about  $10^{-1} \text{ s}^{-1}$ . Shear yield strength has the same value of 55 kPa for normal applied loads of 150 to 750 kPa. This is similar to Stevens' (1983) results.

Clay has frequently been used in order to simulate faulting in the upper crust (e.g. Oertel 1965). The "clay" used in the present models is a mixture of about 40–50 % by weight water with a commercial talc powder. The yield strength is about  $10^2$ – $10^3$  Pa, which is very close to the previously published values for argillaceous clays.

Dry talc powder is a very suitable material for simulating brittle materials under natural gravity, especially because the progressive development of faults or tension gashes is very similar to that observed in rocks. Dry talc powder is a very soft material under the conditions of tectonic modelling. It was not possible to measure the cohesion in the shear box used for the other materials because of the lack of sufficiently soft dynamometric rings. Comparison with the other experimental materials in the apparatus used for tectonic modelling gives an estimate of the shear strength of about 10 to  $10^2$  Pa.

Dry sand is the most commonly used material in scaled faulting experiments because it has no cohesion. In fact, this is true only for very pure quartz

Table 1. Correspondence between geometrical and mechanical parameters for the basement of the models, rocks, natural basins and a prototype scaled from the models.

	Model	Rocks	Model ratio	Scaled prototype
Length	1 cm	10 km	$10^{-6}$	10 km
Time	3 mn	30 My	$10^{-12}$	30 My
Strain rate (tectonic models)	$10^{-3}$ , $10^{-2}$	$10^{-13}$	$10^{-12}$	$10^{-15}$ , $10^{-14}$
Strain rate (shear tests)	$10^{-1}$	$10^{-15}$		$10^{-13}$
"Yield strength"	$6 \cdot 10^4$ Pa plasticine at $10^{-1} \text{ s}^{-1}$	$10^7$ , $10^8$ Pa at $10^{-13} \text{ s}^{-1}$	$10^{-3}$ , $10^{-2}$	
	$10^2$ , $10^3$ Pa (clay)	(Dixon & Summers 1985)	$10^{-4}$ , $10^{-6}$	

Table 2. Correspondence between geometrical and mechanical parameters for the upper layer of the models, rocks, natural basins, a prototype scaled from the models and an ideal model scaled from rocks.

	Model	Rocks	Model ratio	Scaled prototype	Ideal scaled model
Length	1 cm	10 km	$10^{-6}$	10 km	1 cm
Layer thickness	5 mm	500 m	$10^{-6}$	5 km	0.5 mm
Grain size	$10^{-5}$ (talc) to $10^{-6}$ m (sand)	$10^{-3}$ to $10^1$ m	$10^{-6}$	10 m to 125 m	$10^{-6}$ mm to $10^{-2}$ mm
Density	$0.65 \text{ g cm}^{-3}$	$2.7 \text{ g cm}^{-3}$	0.25	$2.7 \text{ g cm}^{-3}$	$0.65 \text{ g cm}^{-3}$
Time	3 mn	30 My	$10^{-12}$	30 My	3 mn
Strain rate	$10^{-2} \text{ s}^{-1}$	$10^{-14} \text{ s}^{-1}$	$10^{-12}$	$10^{-14} \text{ s}^{-1}$	$10^{-2} \text{ s}^{-1}$
Cohesion		$10^7$ Pa	$0.25 \cdot 10^{-6}$		2.5 Pa
"Yield strength" (Dry talc powder)	$10^1$ to $10^2$ Pa*	$10^7$ to $10^8$ Pa*	$0.25 \cdot 10^{-6}$	$4 \cdot 10^7$ to $4 \cdot 10^8$ Pa	2.5 to 25 Pa

(\* : estimated from the tectonic models ; \* : after Dixon & Summers, 1985)

sand and the presence of clay minerals causes cohesion to appear. However, this cohesion has been found too small to be measured and has been considered to be negligible. The grain size of the sands we used is 125 micrometres.

Tables 1 and 2 give the geometrical and mechanical parameters for basement and cover respectively. Because of the definition of the models, stresses due to gravity need not be scaled in basement if the relative displacement along the faults and the strain at their tips is to be analysed only qualitatively. However, it is essential to take them into account in the cover where structures due to gravity are studied. Note that grain size used for sand corresponds to detrital blocks much larger than the average size observed in natural basins. This seems of minor importance in the present experiments because the mechanism of transport and the geometry of deposition structures are roughly the same for blocks of more than some centimetres regardless of the actual size of the blocks (only the transport distances differ in nature).

Models

Three types of models were used:

– Type 1 models are tests of a cover above rigid basement with a master fault parallel to the shear

plane. This was done by simply depositing a 1 cm thick layer of clay or dry talc directly above the sliding plates. 67 model experiments were carried out with dry talc and 18 with clay.

– Type 2 models are tests of a cover above ductile basement with no discontinuities. In these models a 1 cm thick layer of clay was deposited over a silicone putty slab which deforms almost homogeneously at the strain rates we used and show little boundary effects (type 2 models had wider shear zones than type 1 models). 11 model experiments were carried out.

– Type 3 models are tests of basement with variously trending discontinuities. Dry talc is too soft to cut sections. However, the Riedel fractures formed at any given time may be considered – and will behave – as pre-existing faults with respect to the subsequent strain increments. In all the runs, it is then possible to study the behaviour of pre-existing faults situated within the shortening field, i.e. faults at angles between 0 and +90° to the shear plane. Faults situated in the elongation field, i.e. at angles between +90° and +180° to the shear plane, were created by pre-shearing the model in the opposite sense (e.g. fig. 4). In clay models, both procedures were used. In plasticine models, pre-existing "faults" are hand-made cuts and the behaviour of 139 individual "faults" with various trends were analysed in 62 models. Models with intersecting faults were not investigated in this class of models. Experiments with pre-existing faults focused on five processes: the rotations of the "faults" in the different experimental materials; the sense of strike-slip displacement along them; deformation at their ends; dip-slip motion associated with the strike-slip motion; and the occurrence and amount of opening as a function of fault trend.

– Type 4 models were similar to type 3 models with covers of dry sand or dry talc, but intersecting faults were also considered. For convenience, plasticine basements have been used in most of the experiments. Clay basements were tested but were abandoned because water frequently diffused into the cover. However, the few models which were run gave results similar to plasticine.

## Results.

### *Type 1 models*

Type 1 models with dry talc have been partly described previously (Deramond et al. 1983, Soula 1984) and are reviewed only briefly here. The most interesting result is the development of primary and secondary Riedel shears. Primary Riedel shears

(PRS) correspond to the usual Riedel shears observed by e.g. Wilcox et al. (1973), i.e. conjugate faults with acute bisectrices at 45° to the shear plane. Secondary Riedel shears (SRS) are conjugate shears associated with acute bisectrices at 45° to PRS. During the early stages (overall gamma value smaller than 0.05) the development of PRS is predated by the development of en échelons SRS along the potential PRS which are still shear zones and not fractures. However, shearing prior to the development of PRS is small (local gamma value smaller than 0.1). The angles between the principal compressive stress and the PRS were measured in 67 model experiments. The arithmetic mean is 33° which is similar to the values measured in both previous clay experiments and in rocks. Primary and secondary tension gashes at 45° to the master shear plane and to the PRS respectively are also observed (fig. 5 in Soula 1984). With larger shearing (overall gamma values greater than 0.3) the development of alternating pull-apart and push-up structures is observed (Fig. 1a). Pull-apart "basins" form along open Riedel shears or tension gashes and their development is enhanced by interference between these faults. (Fig. 1). Push-ups are responsible for uplifts similar to those observed in other model experiments (e.g. Groshong and Rodgers 1978). As a rule, the behaviour of dry talc is very brittle: ductile deformation before faulting is negligible and the shortening occurring within the push-ups is accommodated by thrusting with sub-horizontal thrusts (t in Fig. 1a).

Type 1 models with clay give results roughly similar to those obtained in dry talc and in other clay models (e.g. Wilcox et al. 1973). Conjugate primary Riedel shears with acute bisectrices at 45° to the shear plane, and tension gashes also at 45° to this shear plane, are similar to those observed in dry talc. Secondary Riedel shears also developed but rarely as arrays of en échelon faults predating the PRS. The angle between the principal compressive stress and the faults is very similar to dry talc with an arithmetic mean of 31°. Clay is more ductile than dry talc and folding is observed before faulting. Alternating pull-apart and push-up structures also formed but shortening is accommodated in the push-ups by folding instead of thrusting. The apertures often have triangular shapes and the largest initiate where a Riedel shear cross-cuts fractures parallel to the master shear plane (Figs. 1b, c). In both clay and talc type 1 models, the push-up and pull-apart structures are rather similar to those predicted by Rodgers' (1980) numerical models for infinitesimal strain. However, the orientation of faults differ from those shown by Rodgers and no normal fault formed at more than 90° to the shear plane.

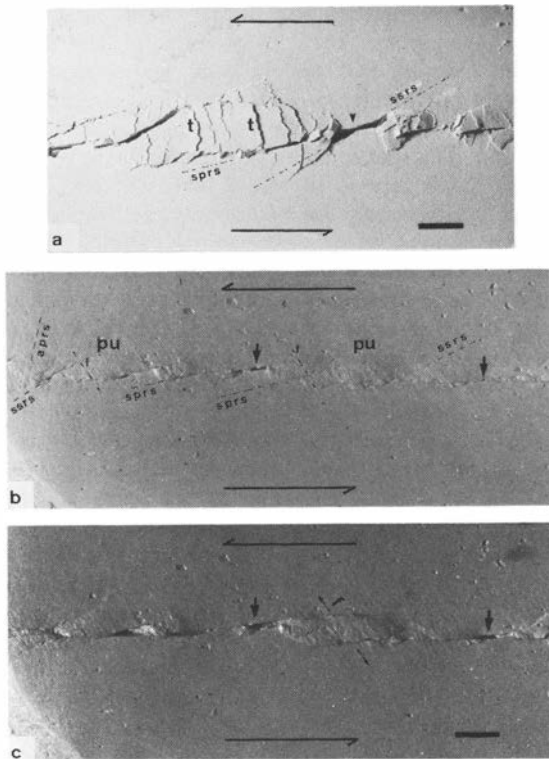


**Fig. 1.**  
 a) Type 1 model with dry talc.  $\gamma = 0.4$ . Development of a triangular pull-apart basin at a junction between secondary and primary Riedel shears (arrow). sprs = synthetic primary Riedel shear; ssrs = synthetic secondary Riedel shear; t = thrust sheets with shallow dips verging to the right. Scale bar is 1 cm.  
 b, c) Type 2 model with clay. In a:  $\gamma = 0.2$ ; in b:  $\gamma = 0.35$ . Development of triangular pull-apart basins at junctions between secondary and primary Riedel shears (arrows), alternating with push-ups (pu). sprs = synthetic primary Riedel shears; aprs = antithetic primary Riedel shears; ssrs = synthetic secondary Riedel shears; f = folds. Note that the folds axes in the push-ups are at  $60^\circ$  to the shear plane in (a) and at  $65^\circ$  in (b) and developed as a result of the local deformation in the push-ups. Scale bar is 1 cm.

This discrepancy might be only apparent since Rodgers assumes, for convenience, that shear failure occurs at an angle of  $\pm 45^\circ$  to the most compressive principal stress axis and not at angles between  $20\text{--}40^\circ$  as observed in rocks and in the present experiments.

Type 1 models with plasticine show a much larger amount of ductile deformation before faulting. In the conditions of modelling, faulting is observed only in thin sheets (thinner than 0.3 cm) and after a shear strain greater than 0.4–0.5 (cf. Soula 1984 fig. 2).

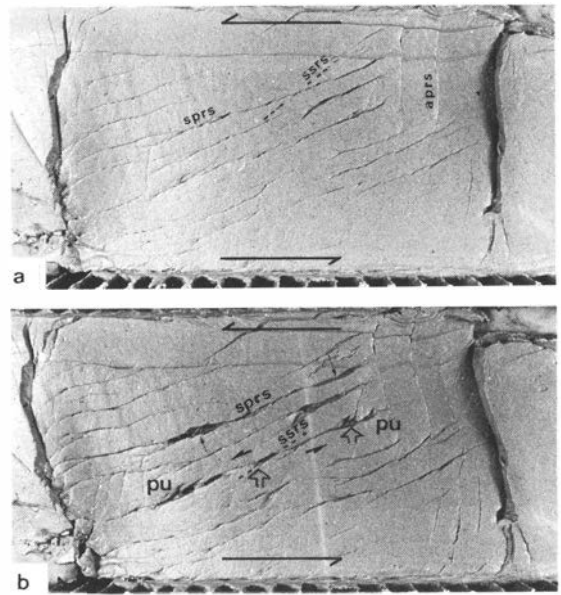


**Fig. 2.** Type 2 model with clay cover above a silicone putty basement with no preexisting faults. Shear strain,  $\gamma = 1$  in (a) and  $\gamma = 1.25$  in (b). The conjugate primary Riedel shear initiated  $13^\circ$  and  $78^\circ$  to the shear plane. Note dip-slip motion associated with push-ups (pu) at fault tips (lowered side arrowed) and opening at junctions between primary and secondary shears (open arrows). sprs = synthetic primary Riedel shears; aprs = antithetic primary Riedel shears; ssrs = synthetic secondary Riedel shears.

### Type 2 models

Type 2 models show fault patterns similar to type 1 models but, because of the almost homogeneous deformation of basement, the shear zone is not localised in the central part of the model but develops over its complete width. The angles of faults with the shear plane are the same as in type 1 models with clay. With progressing shear, the fractures rotate and the high angle antithetic Riedel shears show a much larger rotation than the low angle synthetic Riedel shears and the antithetic relative displacement is well marked (Fig. 2a, b).

### Type 3 models

Type 3 models give results qualitatively similar for all tested materials.

The rotation of the fractures is obvious in plasticine models where all 139 faults rotated in the same sense as the bulk shear. The rotation is slower than that of passive marker lines for faults at angles to the shear plane less than  $-45^\circ$  and more than  $+135^\circ$  and faster for faults between  $+45^\circ$  and

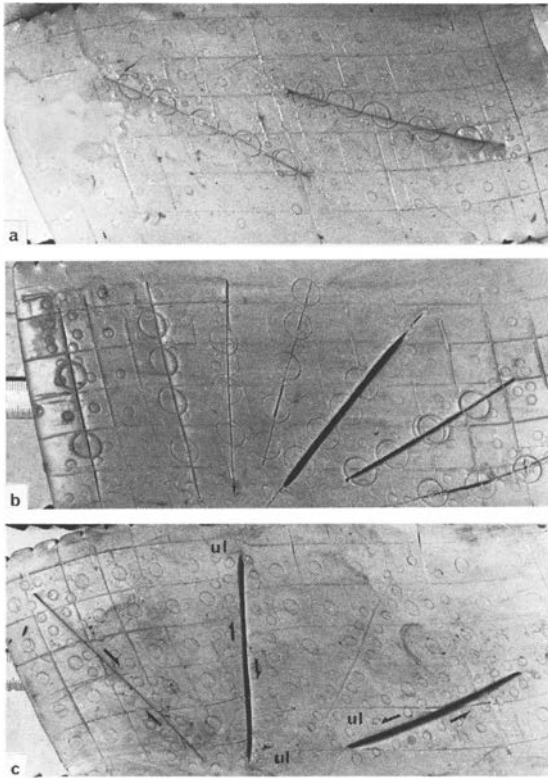


*Fig. 3.* Type 3 models in plasticine. Shear strain,  $\gamma = 0.35$  in (a),  $\gamma = 0.2$  in (b) and  $\gamma = 0.45$  in (c). Relative displacement is antithetic for faults at angles between  $+45^\circ$  and  $+135^\circ$  to the plane and synthetic for the others. Relative displacement is small for faults at an angle of about  $45^\circ$  to the shear plane, and shortening parallel to the fault is dominant (third fault from the right in b). In (c), strain ellipses show shortening on the leading edges on both sides of the faults (first and second faults from the right) with uplifts (ul) and dip-slip motion.

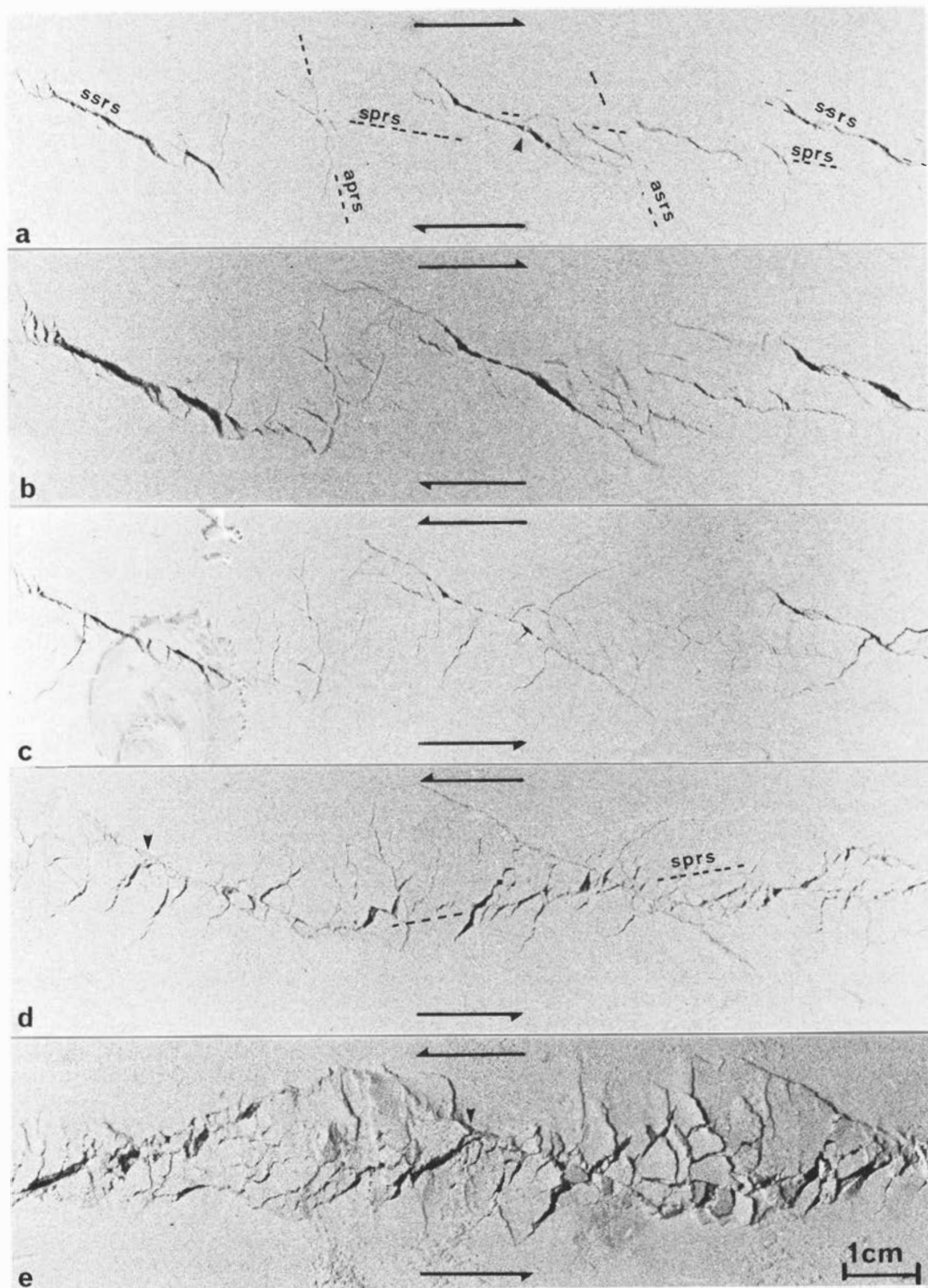
$+135^\circ$  (Fig. 3). This is less apparent for faults at angles greater than  $+90^\circ$  because the compression perpendicular to the faults makes sliding parallel to the faults less easy. However, the difference in finite rotation between "faults" and passive marker lines does not exceed  $10^\circ$  for a shear strain of 1. The finite rotation is less in clay models than in plasticine models for a same bulk shear strain in all types of models. This rotation is similar to that observed in plasticine for the early ductile stages of the deformation. It is smaller in the late stages when the

pull-apart structures and displacement parallel to the shear plane became prominent. The finite rotation in dry talc models is still less than in clay models but the faults also rotate with progressing shearing, except in the very late stages of the deformation. The rotation with progressing shear of fractures which formed in type 2 models is consistent with type 3 models. As a consequence of rotation, a certain amount of either shortening parallel and extension perpendicular to the fractures, or extension parallel and shortening perpendicular to the fractures, opens or closes the fractures (Figs. 2 and 3). Plasticine models obviously exaggerate this effect because the rocks in the uppermost crust are more brittle. However, this effect is also present in clay – which has a behaviour very similar to rocks – and in dry talc which has a behaviour at least as brittle as the most brittle rocks in nature (compare, for example, the results of the present experiments with the development of tension gashes in rocks). Therefore, this effect has to be taken into account when studying the development of natural basins. It is also of some importance because most previous models for the opening of basins seem to consider only pull-apart due to displacement parallel to the shear plane (e.g. Ballance & Reading 1980). The models reported here show that pull-apart opening is present in the more brittle materials but that a component of local shortening parallel, and local extension perpendicular, to the faults is partly responsible for the opening of the faults in any material. Incidentally, this shows that basement structures responsible for the development of basins cannot be accurately simulated if basement is simulated by rigid materials (e.g. wooden blocks).

The sense of strike-slip displacement along finite faults is practically the same as for infinitesimal strain. This can be shown statistically for plasticine models where the displacements are the largest: of the 139 "faults" shown in Figure 5, only 21 faults (trending at angles between  $+20^\circ$  and  $+35^\circ$  to the shear plane) rotated in a sense opposite to that of infinitesimal strain. In all the experiments performed with clay and dry talc, the sense of finite displacements was the same as the infinitesimal displacement.

Deformation at fault tips is clear in all materials. The relative displacement along the faults is accommodated on each side by a shortening at the leading edge and an extension at the trailing edge. This is

*Fig. 4* Type 3 models with dry talc. Left-lateral shear strain,  $\gamma = 0.05$  in (a) and  $\gamma = 0.08$  in (b). Right-lateral shear strain,  $\gamma = 0.1$  in (c),  $\gamma = 0.15$  in (d) and  $\gamma = 0.65$  in (e). Same key as Figs. 1 and 2. In (a) and (b), note the development of echelon secondary Riedel shears along a potential primary Riedel shear to the right of the picture. The triangular mark in (d) and (e) shows the same point. Note that the pre-existing NW trending shears act as reverse faults in (e).



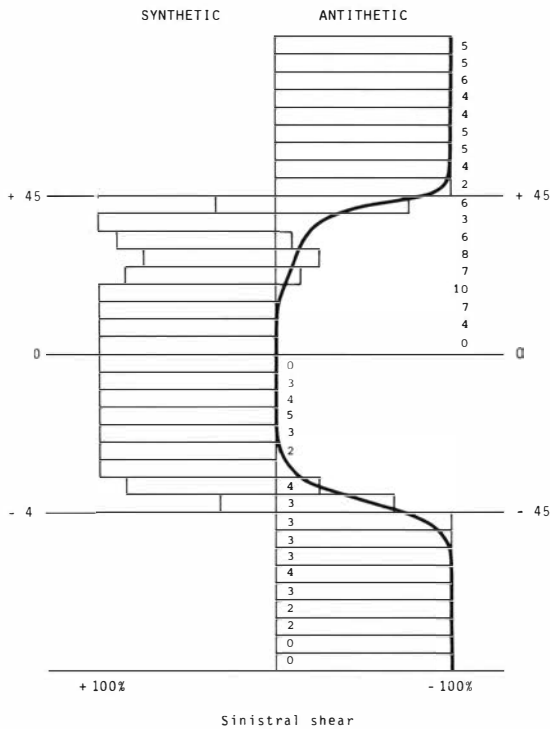


Fig. 5. Sense of displacement observed along pre-existing faults in plasticine models. The angle between the shear plane and the initial orientation of the fault is on the ordinate axis. For convenience, it has been noted as positive when it was synthetic and negative when it was antithetic (an angle of  $-45^\circ$  corresponds to an angle of  $+135^\circ$ ). The percentages on the abscissa are for each orientation class. The small numbers are the numbers of faults which have been measured for each orientation class.

especially clear in plasticine models where ductile behaviour allows large straining without fracturing (Fig. 3) but is also seen in type 2 clay models (Fig. 2). Deformation at fault tips explains why finite displacement is in the same sense as infinitesimal displacement: in materials with oblique pre-existing discontinuities two mechanisms may cause relative displacement: 1) "block rotation", i.e. rotation of the blocks situated between two adjacent discontinuities, eventually associated with internal ductile deformation, giving rise to relative displacement along the discontinuities with senses systematically opposite to that of bulk shear (Wilcox's 1973 internal rotation) and 2) the addition of infinitesimal displacements, i.e. the integration of the displacements related to infinitesimal strain. Because the faults have finite lengths, the latter mechanism is possible only if displacement is accommodated by ductile strain (with surface changes). Clear evidence of this mechanism is given by plasticine models. Block

rotation was small or absent in the present experiments. In fact, block rotation is observed qualitatively in plasticine or clay models but the relative displacement along the faults related to it is small compared to the finite displacement. The relative displacement related to block rotation is more important in plasticine or clay models where interference effects occur between intersecting faults (Soula et al., 1979; Soula 1984). The present study shows that block rotation cannot be generalized to situations without interfering faults. Rotation of entirely rigid blocks can only lead to an increase in width of the shear zones if the boundaries to the rigid blocks are at angles between  $0$  and  $+90^\circ$  to the shear plane; the shear zone decreases in width if these are at angles between  $+90^\circ$  and  $+180^\circ$  to the shear plane. This emphasises that basements to sedimentary basins cannot be accurately simulated by rigid materials such as wooden blocks, because in this case, only motions parallel to the master shear plane are possible.

Dip-slip motions are observed in all models. They are a consequence of the uplift of the compressed zone and depression of the extended zone at fault tips and are systematically associated with the strike-slip motions. As one might expect, the values of dip-slip displacement appear to be functions of the local strain along the fault and vary with the length of the faults, with the value of strike-slip displacement and with the concentration of strain along the fault. Because of the interaction of these factors, it has not been possible to study statistically the role of each process. However, in plasticine dip-slip motion is greater for "short" (1 to 2 cm long) faults than for "long" (3 to 5 cm long) faults with values of about 2 to 3 mm and 1 mm respectively, for a gamma value of about 0.3–0.4 and initial angle to the shear plane between  $60$  and  $75^\circ$ . In any event, because deformation at fault ends is necessary for strike-slip displacements to occur, dip-slip motion is necessarily associated with strike-slip motion with uplifted zones facing depressed zones at fault ends (Figs. 2 & 3). Recognition of such uplifted and depressed zones at fault ends may be a useful shear criterion in sedimentary basins.

The opening of the faults is essentially due to two mechanisms (Fig. 6). The first possible mechanism is a displacement parallel to the shear plane which opens faults (or sections of non-linear faults) oblique to the shear plane acting as relays between faults parallel to the shear plane (or between en échelon faults along which there is a strike-slip displacement without noticeable opening). This mechanism is well documented in the literature (e.g. Bal- lance & Reading 1980 or Gamond 1985) and very often thought to account for pull-apart structures.

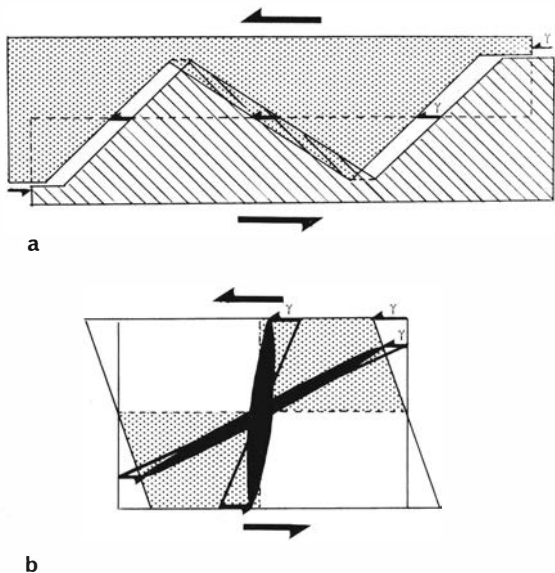


Fig. 6. Possible mechanisms of opening pre-existing faults. (a) Pull-apart as a result of relative displacement parallel to the bulk shear plane. (b) Opening due to compression parallel, and extension perpendicular, to the faults as a result of their rotation within the extension field of the infinitesimal strain ellipse (stippled area). The initial orientation of open faults is shown by thick lines.

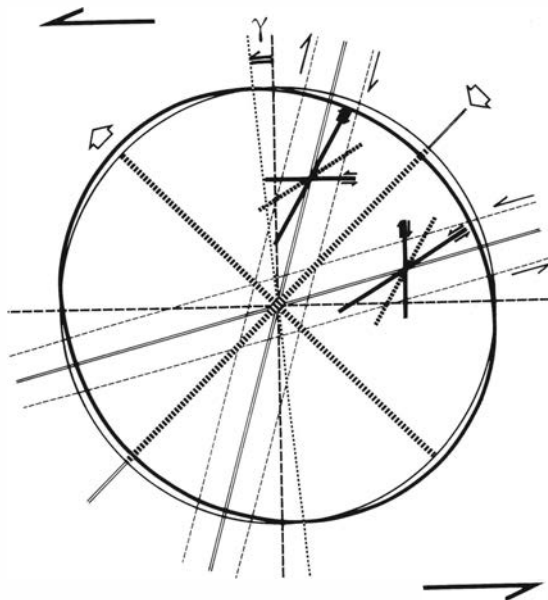


Fig. 7. Development of Riedel shears with respect to the infinitesimal strain ellipse. Thick continuous lines are secondary Riedel shears with acute bisectrix at  $45^\circ$  to the primary Riedel shears. Double lines are primary Riedel shears. Thin interrupted lines show the boundaries of the shear zones corresponding to the potential primary Riedel shears before rupture.

For convenience, it will be referred to as pull-apart in the remainder of the present paper. Alternatively, opening may be the result of shortening parallel, and extension perpendicular, to faults situated within the extensional field of overall strain. In simple shear, this is the case of faults rotating within the infinitesimal extension field, i.e. faults with initial and final trends at angles between  $0^\circ$  and  $+90^\circ$  to the shear plane.

In plasticine models, opening of the faults occurs essentially as a result of their rotation within the shortening field. Conversely, in the extension field, the faults close because of the combination of extension parallel to them and shortening perpendicular to them. Pull-apart only occurs where there are intersecting faults (see Soula 1984 fig. 4 b).

In dry talc and clay experiments, opening is mainly due to pull-apart parallel to the master shear plane. However, some shortening always occurs due to the rotation of the faults. This is especially clear in clay models where there is a noticeable rotation before pull-apart becomes dominant (Fig. 1b, c). This is observed also in dry talc where the rotation is much smaller. In fact, in both talc and clay models, careful observation shows that pull-apart occurs only where two or more intersecting faults are pres-

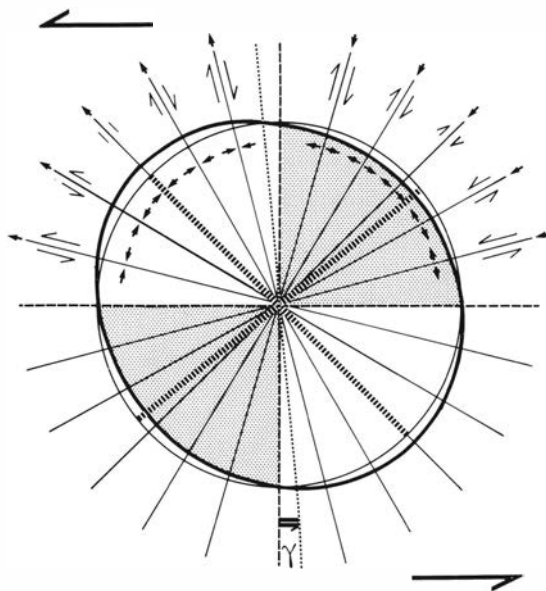


Fig. 8. Displacement and deformation along variously trending pre-existing faults with small finite shearing. The thin half-arrows show relative displacement. The small thick arrows show the compression or extension parallel or perpendicular to the faults. Stippled area is the shortening field of the infinitesimal strain ellipse.

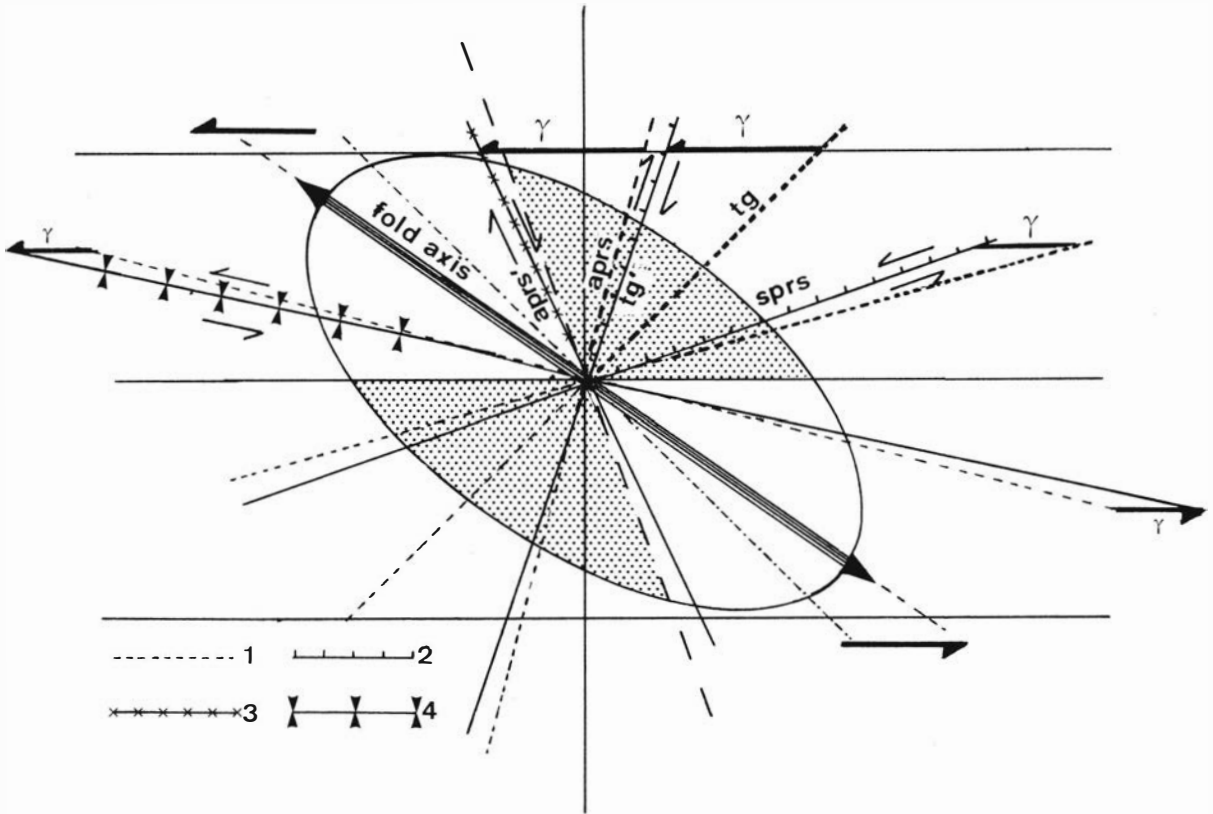


Fig. 9. Behaviour of primary Riedel shears after large shearing. Shear strain,  $\gamma = 0.7$ . (1) = initial orientation of fractures; (2) = fractures acting as normal faults; (3) = fractures which opened and then closed when passing from the shortening field to the extension field; (4) = closed faults possibly acting as reverse faults; sprs = synthetic primary Riedel shears; aprs = antithetic primary Riedel shears, initial orientation; aprs = antithetic primary Riedel shears, final orientation; tg = tension gashes, initial orientation; tg' = tension gashes, final orientation; stippled area = shortening field of the finite strain ellipse.

ent (Figs. 1, 2 4a). It seems then that one of the reasons why pull-apart rapidly becomes dominant in clay and talc is that no isolated faults form in these materials.

In any event, the experiments show that only faults situated within the shortening field of the infinitesimal strain open, even though the opening is mainly due to pull-apart parallel to the master shear plane. In the same way, all the faults initially situated within the extension field will close. Figures 7, 8 and 9 show a synthesis of the results of type 1, type 2 and type 3 models.

#### Type 4 models

Type 4 models have been already described in previous papers (Soula et al. 1979, Soula 1984). In these preliminary models, structures similar to sedi-

mentary basins were duplicated in the cover above open faults. In the more brittle cover materials such as dry talc, "sedimentation" was marked by collapse of rhombohedral fragments of various size along normal listric faults, giving rise to lozenge-shaped "basins". Less cohesive materials such quartz-rich sand developed debris cones symmetrically disposed about the axis of the structure, duplicating natural lateral debris cones or alluvial fans on both sides of a drainage axis. These models also showed systematic characteristics: (1) basins in the cover were considerably wider than the opening of the fault in basement; (2) the faults which developed in the cover were essentially normal faults even though the faults in the basement acted as strike-slip faults; (3) conjugate fault systems in the cover had an acute bisectrix parallel to the open basement faults trending at angle between  $0^\circ$  and  $+90^\circ$  to the overall

shear plane; (4) normal faults developed in several successive generations during progressive strain and sedimentation was progressive, as frequently observed in natural basins.

The present experiments permit refinement of the preliminary findings (Soula 1984). The most important refinement concerns the mechanisms of opening of basins. Basins form only above basement faults in the shortening field, regardless of how they open. The deformation in the basin over the fault is a combination of several mechanisms: i) shortening parallel to the fault occurs by conjugate cover faults with acute bisectrices parallel to the basement fault, ii) strike-slip simple shear parallel to the basement fault is responsible for Riedel fractures and tension gashes in the cover, iii) extension perpendicular to the basement fault results in extensional normal cover faults or reactivation of previously formed cover faults and iv) dip-slip motions at the tips of the basement faults. The prominence of one or other of these mechanisms depends essentially on the original trend of the basement fault and on the shear value. Shortening parallel to the basement fault, with normal or conjugate faults with acute bisectrices also parallel to it, is prominent for faults with trends close to  $45^\circ$  to the shear plane. Structures develop similar to those observed in pure extensional models, i.e. extensional normal faults, tilted blocks etc. Pull-apart and push-up structures similar to those observed above the master shear plane in single layer models form only above faults at low angles (less than  $10-15^\circ$ ) to the master shear plane. Therefore, the morphologic and tectonic structures observed in the experimental basins (Fig. 10) are, in some cases, similar to structures frequently described in basins formed in strike-slip zones. Examples of these are rhombohedral or parallelogram shapes of basins or of sub-basins, oblique margins of the basins and transport of deposits parallel to the strike-slip faults. Others, however, show no marked differences with structures observed in purely extensional basins such as dip-slip faults, tilted blocks, listric faults, symmetrical arrangement of debris cones, and conjugate faults. This may be explained by the fact that there is always a component of extension perpendicular to the basement fault along which the "basin" develops, especially when taking into account the fact that "basins" form only along fractures in the extension field. However the ratio between the extensional component perpendicular to the basement fault and of strike-slip simple shear component parallel to it vary as a function of the trend of the fault with respect to the master shear plane. The component of infinitesimal strike-slip simple shear is minimum for faults at angles close to  $45^\circ$  to the shear plane and vanishes

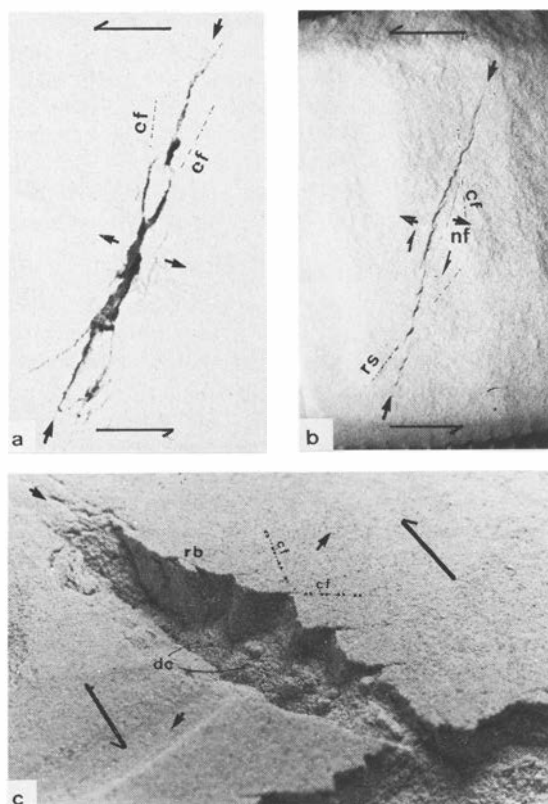


Fig. 10. Type 4 models, structures in the cover above a basement fault. (a) Dry talc cover. Shear strain,  $\gamma = 0.35$ . Symmetrical arrangement of the fractures with collapsing rhombohedral or triangular blocks. (b) Micaeous sand. Shear strain,  $\gamma = 0.25$ . Development of Riedel shears, conjugate faults and normal faults parallel to the basement fault. (c) Mica-poor sand. Shear strain,  $\gamma = 0.4$ . Development of conjugate faults which then acted as normal faults with collapsing rhombohedral blocks. Debris cones formed at the intersection of conjugate faults. In all pictures: cf = conjugate faults; rs = Riedel shears; rb = rhombohedral blocks; dc = debris cones. The thick arrows show the direction of local shortening or extension.

at  $45^\circ$ , whereas the component of infinitesimal extension is maximum for the same angle of  $45^\circ$ . This explains why symmetrical depositional arrangements and tectonic structures are observed for basement faults trending at angles close to  $45^\circ$  to the master shear plane (Lucas 1985 figs. 8 and 35).

An important result of the experimental models above is the fact that no normal (extensional) fault can form at angles between  $90^\circ$  and  $180^\circ$  to the shear plane and that no pre-existing faults with such initial orientations can open or act as normal faults. Conceptual models involving pull-apart basin development along or with faults at angles greater than

+ 90° to the master shear plane (i.e. within the extension field) are not consistent with the present model experiments, regardless of the origin of the faults or the boundary conditions. As far as we are aware, no previous experimental works supported such conceptions (e.g. Wilcox et al. 1973 or Gamond 1985). Nevertheless, several models were especially designed to test the conceptual models of Crowell (1974, fig. 3) or Steel & Gloppen (1980, fig. 14) widely accepted amongst sedimentologists. The resulting structures were similar to those described above and it was impossible to obtain the structures predicted by the authors with the mechanisms and initial conditions they envisage.

Another important result is the development of uplifts and depressions at the leading and trailing edges, diametrically opposed on either side of the faults. Even though not observed in the cover of model experiments, the recognition of uplifted and depressed zones is one of the most important criteria for determining the sense of shear along strike-slip related basins. Taking into account the effects of erosion, possible sedimentary patterns which are likely to result from these structures are shown in Figure 11.

The structures observed in the cover are diagnostic only for faults at a low angle to the shear plane. However, when considering a population of faults (and/or basins with differing trends) rather than single faults (and/or basins), it will be possible to recognize strike-slip systems if the orientations of basins and extensional syn-sedimentary faults permit determination of the shortening and extension fields of the strain ellipsoid (Figs. 8 and 9).

A point not taken into account in the models is that natural basins might develop from faults in the extension field because of rivers preferentially devel-

oped along fault zones which are less resistant to erosion than the surrounding material. However, in this case, neither extensional tectonic structures parallel to the fault within the basin, nor deposition structures related to extensional structures in the bed rocks (e.g. tilted blocks or collapsed rhomboidal blocks) will be observed.

### Comparison to the Bierzo basin (NW Spain)

The post-Pyrenean Miocene Bierzo basin in NW Spain (Fig. 12) has been selected for comparison with some of the models presented here. A detailed sedimentological, geomorphological and structural study of this basin is reported in Herail (1983). The experimental results above lead us to refine the earlier interpretations (Herail 1983) and suggest a regional structural model for NW Spain.

The Bierzo basin is the easternmost inter-mountain Miocene basin of the Galician-Leonese massif. To the west, it is connected with the basins of central Galicia through the Rubiana basin and smaller

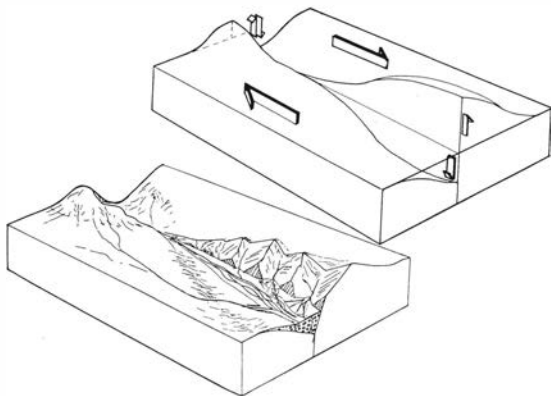


Fig. 11. Block diagram of possible deposition structures and morphology associated with the deformation at fault tips. The asymmetry will result from the asymmetry of the slopes on both sides of the fault.

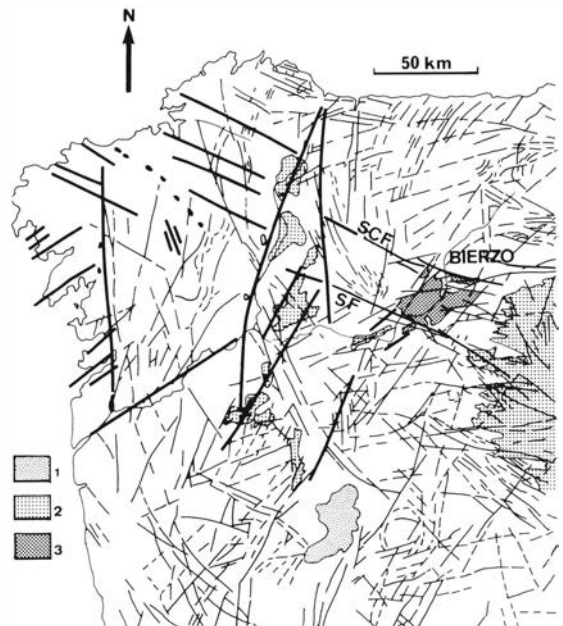


Fig. 12. Location of the Bierzo basin with respect to the principal faults in NW Spain. The thin lines are from Lansat imagery (IFP-CNEXO 1976). The thick lines are from the seismo-tectonic map of Spain. Line with intermediate thickness are faults which have been recognized from field studies. The faults from Lansat imagery have been confirmed by field examination in the Bierzo area. SCF = South Cantabric fault zone; SF = Sil fault. (1) Santalla Formation; (2) Miocene uplift; (3) Undifferentiated Santalla & Las Medulas formations.

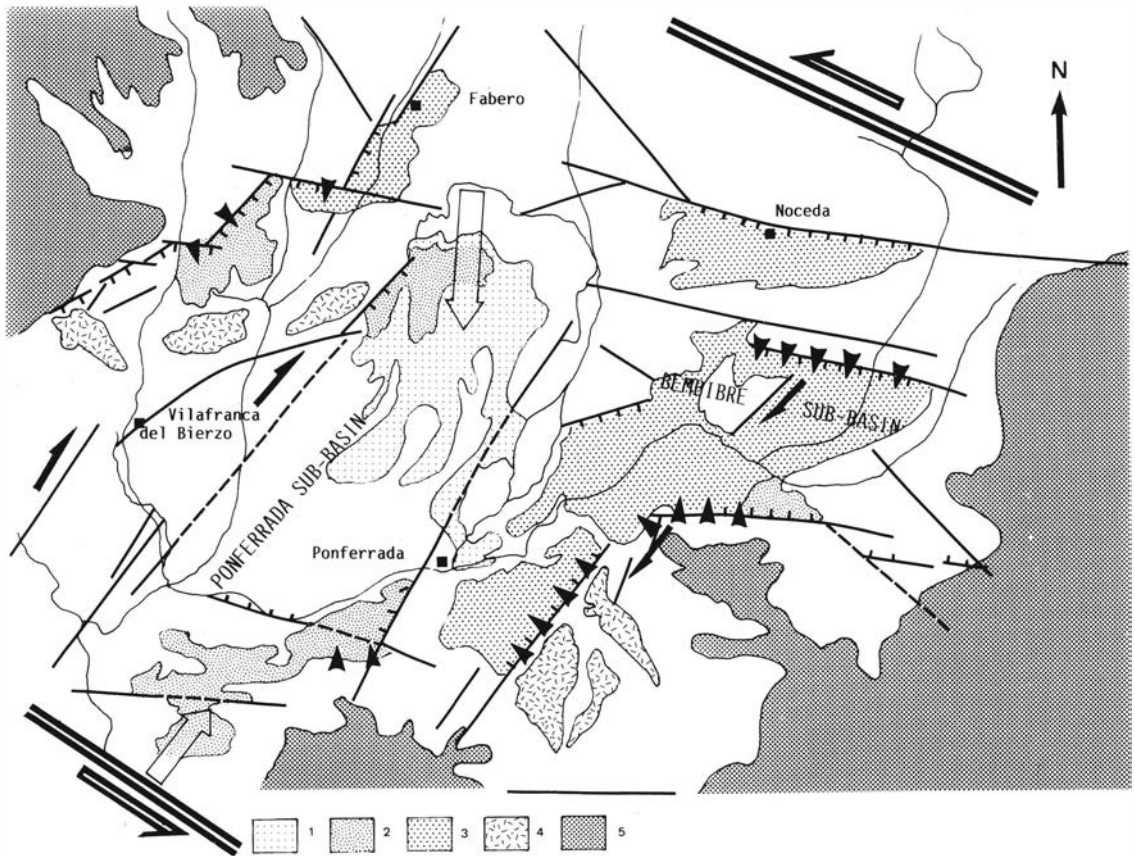


Fig. 13. Bierzo basin. Structure and origin of the materials constituting the Santalla and Las Medulas formations. (1) Santalla Formation; (2) Las Medulas Formation; (3) Undifferentiated Santalla and Las Medulas formations, (4) Uplifted areas eroded before the deposition of the plateau conglomerates; (5) Miocene uplifts. The open arrows show directions of the principal rivers. Solid arrows show the origin and directions of local deposits. The double thick lines represent the overall trend of the major regional faults (South Cantabric and Sil faults); the sense of shear in inferred from the structures within the basin.

basins arranged along the Sil and Bibey valleys. To the East, the most recent deposits of the Bierzo basin are related to those of the North-West of the Duero basin. As a whole, the Hesperic massif was affected by an important late-Hercynian faulting (e.g. Parga 1969, Marcos 1973, Perez Estaun 1973, Arthaud & Matte 1975). The late-Hercynian faults were reactivated later, especially during the Cainozoic (Herail 1983). Figure 12 shows the large-scale fault pattern taken from the seismo-tectonic map of Spain and from a Landsat imagery study by IFP-Cnexo (1976).

The basin formed during a short period during the Miocene: the sedimentary units which characterize the basin, the Santallas and Las Medulas formations, unconformably overlie the Toral Formation which represents a part of a widespread sedimentary series. They are unconformably overlain

by a flat lying formation of plateau conglomerates which has no special regional name. In the Santalla and Las Medulas formations, sedimentation is clearly associated with fault activity: the sediments were derived locally and originated from the fault zones as shown by their composition and the directions of palaeocurrents; the coarser deposits are found against faults acting as normal faults, with lateral debris cones spreading from them (Herail 1983); faults belonging to a same system formed progressively during the deposition as shown by the fact that, at any level of Santallas and Las Medulas formations, the faults deformed part of the previously deposited sediments and were covered by later deposits of the same unit. In the Toral Formation, deposits have a more distant origin and the sedimentation shows no relation with the faults.

Two sub-basins may be distinguished within the

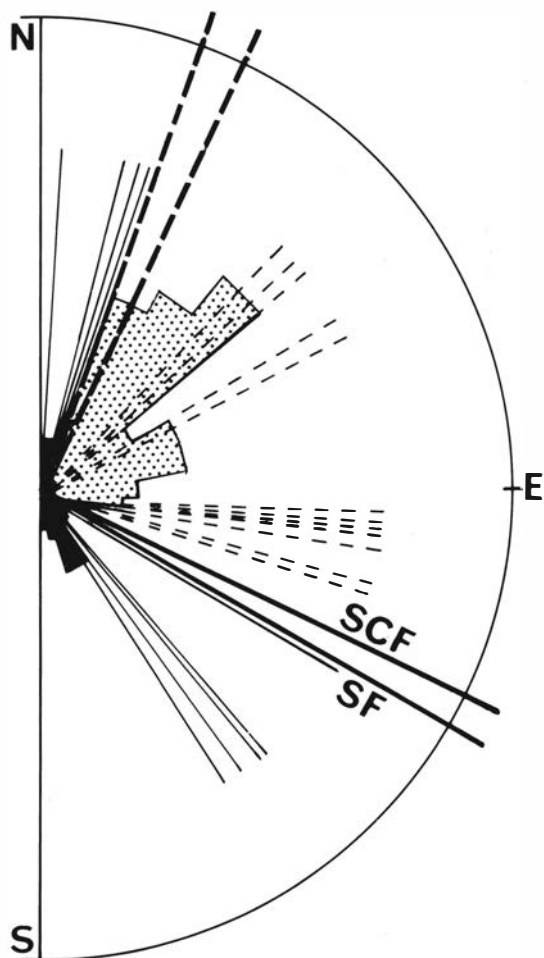


Fig. 14. Orientation of faults in the Bierzo area. The rose diagram show the mesoscopic and medium sized faults (with length between 100 m and 1 km). Stippled area = extensional synsedimentary faults; black area: reverse faults. The lines added on the diagram show the regional faults (each line represents 1 fault). The interrupted lines are the extensional synsedimentary faults and the continuous lines the reverse or wrench faults not open during sedimentation. The thick continuous lines show the orientation of the major regional faults (SCF = South Cantabric Fault; SF = Sil Fault) and the thick interrupted lines show the perpendicular to them.

Bierzo basin: the major NE-SW trending Ponferrada sub-basin, which corresponds to the deepest trough, and the E-W trending Bembibre sub-basin (Fig. 13). Secondary troughs are observed to the north of the Bembibre sub-basin with E-W trend (Noceda) and to the north-west of Ponferrada sub-basin with NE-SW trend (Fabero).

The basement of the Bierzo basin is composed of Palaeozoic sediments unconformably covered by

Stephanian sandstones and is affected by numerous reactivated late Hercynian faults. Field and aerial photo structural studies show that there are two major basement faults with N 115–120 E trends, the South Cantabrian and Sil faults. Other important preexisting regional faults with NE-SW, ENE-WSW to E-W and NW-SE to NNW-SSE trends are also observed (Herail 1983) (Figs. 13 and 14). Other map-scale faults with N-S to NNE-SSW trends are also observed. Statistical study of smaller faults, i.e. with lengths ranging from 100 m to 1 km, gives maxima for N20–50 E, N 70 E and N 140 E (Fig. 14). These field data are consistent with large-scale fault patterns of NW Spain (Figs. 12) which show that the dominant lineaments have N 115 E and N 50 E trends in the Bierzo area. Most of the faults were reactivated before and after the deposition of the Santallas and Las Medulas formations.

Both Bembibre and Ponferrada sub-basins developed along regional major fault zones with NNW-SSW and E-W trends which we suggest calling the Villafranca-Ponferrada and Bembibre-Noceda fault zones, respectively. The relationship between faulting and sedimentation show that the most important of the faults active during sedimentation parallel the trends of the Ponferrada and Bembibre sub-basins, i.e. N 45–50 E and N 95 E to N 110 E respectively. Other but less important synsedimentary faults trend N 60 E, and N 75 E. In the north-western area, minor synsedimentary faults with N 60 E and N 95 E trends are associated with a major N 50 trending fault. Minor faults which opened or acted as extensional faults during sedimentation of the Santalla and Las Medulas formations, i.e. during opening of the basin, have trends ranging between N 20 E and N 120 E (Fig. 14). No opening or synsedimentary normal faulting has been observed for faults of other orientations and it seems acceptable to assume that the N 20 E to N 120 E represented the shortening field. When considering either the major or the minor faults, the boundaries between the shortening and extension fields correspond to the trend of the South Cantabrian and Sill faults and to the perpendicular to this trend respectively. The location of the major Ponferrada and Bembibre sub-basins along the NE-SW and EW Ponferrada and Bembibre major fault zones show that their development was due to preferred opening of these faults. This is also supported by the directions of the palaeocurrents, local deposits and debris cones which originated from boundary faults parallel to the major faults in both sub-basins (Fig. 13), as observed in experimental models (Fig. 10c). On the north-western side of the Ponferrada sub-basin, near Fabero (Fig. 13), minor synsedimentary faults are oblique to the NE-SW pre-existing fault and not

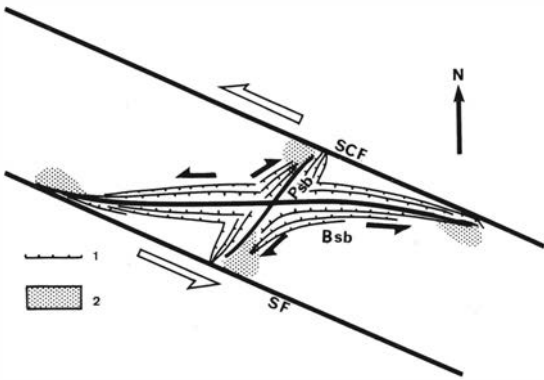


Fig. 15. Schematic interpretation of the Bierzo basin from experimental models. The thick lines represent the basement faults from which developed the Ponferrada and Bembibre sub-basins. Psb = Ponferrada sub-basin; Bsb = Bembibre sub-basin; SCF = South Cantabric Fault; SF = Sil Fault; (1) normal faults parallel to the basement faults; (2) uplifted areas.

in continuity with any major regional preexisting fault. These might be conjugate faults developed during the formation of the basin, similar to those in Figure 10b. They may indicate a compressional component acting in combination with dextral shearing along the Villafranca fault zone similar to cover faults developed in the models (Fig. 10a, b). The best evidence for a component of dextral shearing occurring along the Ponferrada fault is the development of local uplifts north and south of the Ponferrada trough, i.e. at its NW and SW edges. These zones correspond to topographic relief with associated local coarse facies of the Santalla and Las Medulas formations during the opening of the basins. Evidence for this interpretation includes: i) constant sedimentation in the Toral Formation in their vicinity, and ii) the uplifts and the basin are unconformably cut by an erosion surface covered by flat-lying plateau conglomerates. Compared with experimental models, the location of the uplifts on the NW and SE edges of the Ponferrada fault zone can be considered as a result of shortening on the leading edge and extension on the trailing edge on either sides of the fault (see Figs. 2 and 3).

Put together and compared with experimental models (Fig. 3 and 10), the results reported above suggests that the Bierzo basin formed during a large-scale left-lateral strike-slip shearing parallel to the major WNW-ESE trending South Cantabrian and Sil faults acting on major E-W and NNW-SSW faults (Figs. 15 and 16). These allowed dextral

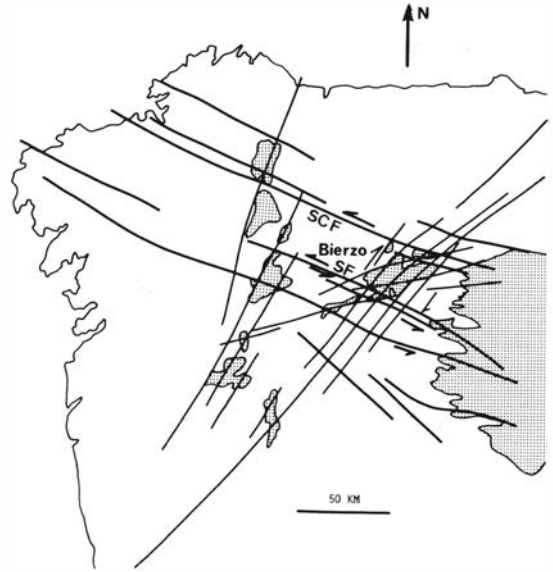


Fig. 16. The formation of the Bierzo basin is attributed to regional sinistral shearing along the major WNW – ESE trending regional faults. Antithetic shearing occurred along NE-SW trending pre-existing faults, and synthetic shearing along ENE-WSW trending pre-existing faults. SCF = South Cantabric Fault; SF = Sil Fault.

shearing along the Ponferrada-Villafranca fault zone which is at an angle of about  $75^\circ$  to the major South Cantabrian and Sil faults. In this interpretation, the major WNW-ESE trending lineament passing through the Bierzo basin may be considered as a wide regional shear zone.

The data on Figure 12 show that the Bierzo basin formed at the junction between this WNW-ESE major fault zone and another major fault zone with NE-SW trend, which could explain the importance of this basin (Fig. 15). It is likely that the left-lateral strike-slip shearing which occurred along the WNW-ESE major fault zone on the scale of the Bierzo basin also occurred along this fault zone on the scale of NW Spain. Most of the other important Miocene basins of NW Spain are situated along regional faults with similar NNW-SSW to NE-SW trends (Fig. 12). This suggests that the interpretation which is proposed for the Bierzo basin could be extended to the other Miocene basins of NW Spain. A more detailed structural and sedimentological study of these basins will be necessary in order to confirm or deny this hypothesis. However, the present study suggests that the model experiments could be used to guide or control these studies.

## General discussion and conclusion

The model described in this paper emphasize the role of pre-existing faults in the control of basin opening, a factor not taken into account during previous model studies. Comparison with natural structures e.g. the Bierzo basin or the Permian and Triassic basins in the Pyrenees (Soula et al. 1979) suggests that such pre-existing faults with differing trends are important in nature and play a major role during basin development in wrench fault zones.

The principal results of the experiments are:

1) Only discontinuities in the infinitesimal shortening field can open. It is not possible for even pull-apart basins to form along discontinuities situated within the infinitesimal extension field whatever the boundary conditions or the internal configuration.

2) Deformation always occurs at the edges of the faults as a result of relative displacement along the faults and is responsible for uplifts. The actual amount of the uplifts is not important. Most important is the fact that they exist and that it is possible to predict their location. Modelling only "simple" situations such as structures developing above the master faults, will have applications limited to only large basins in major fault zones.

3) Ductile materials exaggerate the ductile part of the deformation compared to the more brittle experimental and natural materials, but do not fundamentally change the results. For example, the deformation at fault ends will be accommodated in the more brittle material by thrusting at the leading edge or extensional faulting at the trailing edge. Even so, there will be a shortened zone with a correlative uplift at the leading edge and an elongated zone with a correlative depression at the trailing edge, diametrically opposed on either side of each fault. It is clear that simulating faulted basements by rigid blocks will be much more unrealistic and will give rise to oversimplifications rather than simplifications.

4) Interference between pre-existing faults may considerably affect the behaviour of the basement and of the basins. The development of structures such as pull-apart "basins" is greatly helped or made possible by fault interferences, even in the most brittle materials used in the experiments (dry talc).

The example of the Bierzo basin show that our model experiments may be used as guides for interpreting natural basins. Field data show that some pre-existing faults opened while other closed during sedimentation. Such observations constrain the elongation and shortening fields at this time. Deformation at fault tips caused uplifts and depressions which may be used to determine the sense of rela-

tive strike-slip displacement. The two major sub-basins which constitute the basin developed along NNE-SSW and E-W trending faults situated within the regional shortening field. Comparison with experimental models suggests attributing the development of the basin to a large scale left-lateral shearing along a WNW-ESE trending major fault zone across NW Spain.

The present models cannot aspire to be exact representations of natural structures. This is because erosion or sedimentary processes not directly related to gravity will not be duplicated on the scale of the basins and because the faults extend as normal faults rather than by actual opening. However, gravity-controlled processes such as development of debris cones or alluvial fans, collapse of fault blocks and related structures may be obtained experimentally. Therefore, although the experiments do not predict the exact geometries, they are though capable of predicting the location and the type of depositional structures controlled by tectonic events.

*Acknowledgements.* We thank Jane Gilotti and Chris Mawer for their criticism and suggestions.

## REFERENCES

- Arthaud, F. & Matte, Ph. 1975: Les décrochements tardi-hercyniens du Sud-Ouest de l'Europe. Géométrie et essai de reconstitution des conditions de la déformation. *Tectonophysics*, 25, pp. 139–173.
- Ballance, P.F. & Reading H.G. (editors) 1980: Sedimentation in oblique-slip mobile zones. *Special publication n° 4 of the International Association of Sedimentologists*, Blackwell, Oxford, 265 p.
- Cabrera, L., Roca, E. & Santanach, P. 1988: Basin formation at the end of a strike-slip fault: the Cerdanya Basin (eastern Pyrenees). *Journal of the Geological Society, London*, 145, 8 pp (in press).
- Cloos, E. 1955: Experimental analysis of fracture patterns. *Bull. geol. Soc. Am.*, 66: 241–246.
- Cloos, H. 1928: Experimente zur Inneren Tektonik. *Centr. Mineral., Geol. Paläontol. Abt. B.*: Geol. Paläontol., 609–621.
- Debroas, E.J. 1987: Modèle de bassin triangular à l'intersection de décrochements divergents pour le fossé albo-cénomaniens de la Ballongue (zone nord-pyréenne, France). *Bull. Soc. Géol. France*, 8, t. III, pp. 887–898.
- Déramond, J., Sirieys, P. & Soula, J.C. 1983: Mécanismes de déformation de l'écorce terrestre: structures et anisotropies induites. *5th Congress Intern. Rock Mech., Melbourne*, F 89–93.
- Dixon, J.M. & Summers J.M. 1985: Recent developments in centrifuge modelling of tectonic processes: equipment, model construction techniques and rheology of model materials. *J. Struct. Geol.*, 7, 83–102.
- Gamond, J.F. & Giraud, A. 1982: Identification des zones de failles à l'aide de fractures de second ordre. *Bull. Soc. Geol. Fr.*, XXIV, 4, 755–762.

- Gamond, J.F. 1985: Conditions de formation des zones de discontinuité cinématiques dans la croûte supérieure. Aspects expérimentaux et naturels. Thèse Sc. Grenoble, 196 p.
- Garfunkel, Z., Zak, I. & Freund, R. 1981: Asymetry and basin migration in the Dead Sea rift. *Tectonophysics*, 89, pp. 27–38.
- Groshong, R.H. & Rodgers, M.A. 1978: Left-lateral strike-slip fault model. In: Structural style of Arbuckle region, Geol. Soc. Am., South Central Sect., Field Trip 3, 7 p.
- Heraïl, G. 1983: Géomorphologie et géologie de l'or détritico. Piemonts et bassins intramontagneux du Nord-Ouest de l'Espagne (Monts de Leon, Bierzo). Th. Sc. Toulouse-Mirail, 506 p.
- IFP-CNEXO – 1976: Esquisse photogéologique du domaine méditerranéen. Grands traits structuraux à partir du satellite Landsat 1. Coupure n° 1: Portugal, Espagne, Maroc, Algérie (marge atlantique, mer d'Alboran). Editions Technip, Paris.
- Larouzière, F.D. de, Montenat, C., Ott D'Estevou, P. & Griveaud, Ph. 1987: Evolution simultanée de bassins néogènes en compression et en extension dans un couloir en décrochement: Hinojar et Mazarron (Sud-est de l'Espagne). *Bull. Centres Rech. Explor.-Prod. Elf-Aquitaine*, 11, pp. 23–38.
- Lucas, C. 1985: Le Grès Rouge du versant nord des Pyrénées. Essai sur la géodynamique de dépôts continentaux du Permien au Trias. Th. Sc. Toulouse-Paul Sabatier, 265 p.
- Marcos, A. 1973: Las series del Paleozoico inferior y las estructuras hercinianas del occidente de Asturias (NW de Espana); Trabajos de Geologia, n° 6, 113 p.
- McClay, K.R. 1976: The rheology of plasticine. *Tectonophysics*, 33, 17–115.
- Montenat, C., Ott D'Estevou & Masse, P. 1987: Tectonic-sedimentary characters of the Betic Noegene basins evolving in a crustal transcurrent shear zone (SE Spain). *Bull. Centres Rech. Explor.-Prod. Elf-Aquitaine*, 11, 1–22.
- Perez Estaun, A. 1978: Estratigrafia y estructura de la rama S de la zona Asturoccidental-leonesa. *Memoria IGME Espana*, T 92, 149 p.
- Oertel, G. 1965: The mechanism of faulting in clay experiments. *Tectonophysics*, 2, 343–393.
- Parga, J.R. 1969: Spätvariszische Bruchsystem im hesperischen Massiv. *Geol. Rund.*, 59, pp. 323–336.
- Ramberg, H. 1975a: Particle paths, displacement and progressive strain applicable to rocks. *Tectonophysics*, 28, 1–37.
- Ramberg, H. 1975b: Superposition of homogeneous strain and progressive deformation in rocks. *Bull. Geol. Inst. Univ. Uppsala*, N.S. 6.
- Ramberg, H. 1982: *Gravity, Deformation and the Earth's Crust* (second edition). Academic press, London, 452 p.
- Reading, H.G. 1980: Characteristics and recognition of strike-slip fault systems. in Sedimentation in oblique-slip systems (edited by P.F. Ballance & H.G. Reading). *Spec. Publ. Int. Ass. Sediment.*, 4, pp. 7–26.
- Rodgers, D.A. 1980: Analysis of pull-apart basin development produced by a échelon strike-slip faults. In Sedimentation in oblique-slip systems (edited by P.F. Ballance & H.G. Reading). *Spec. Publ. Int. Ass. Sediment.*, 4, pp. 27–41.
- Soula, J.C. 1984: Genèse de bassins sédimentaires en régime de cisaillement transcurrent: modèles expérimentaux et exemples géologiques. *Bull. Soc. Belge de Géologie*, 93, 83–104.
- Soula, J.C., Lucas, C. & Bessière, G. 1979: Genesis and evolution of Permian and Triassic basins in the Pyrenees by regional strike-slip acting on older Variscan structures: field evidence and experimental models. *Tectonophysics*, 58, T1–T9.
- Steel, R.J. & Gloppen, T.J. 1980: Late Caledonian (Devonian) basin formation, western Norway: signs of strike-slip tectonics during infilling. In Sedimentation in oblique-slip systems (edited by P.F. Ballance & H.G. Reading). *Spec. Publ. Int. Ass. Sediment.*, 4, pp. 79–104.
- Stevens, T.A.C. 1983: A centrifuge study of slope stability using plasticine. unpublished B.Sc. thesis. Queen's University, Ontario.
- Tchalenko, J.S. 1970: Similarities between shear zones of different magnitudes. *Geol. Soc. Am. Bull.*, 81, 6, p. 1625–1640.
- Wilcox, R.E., Harding, T.P. & Seely, D.R. 1973: Basic wrench tectonics. *Bull. Am. Ass. Petrol. Geol.*, 57, 74–96.
- Withjack, M.O. & Jamison, W.R. 1986: Deformation produced by oblique rifting. *Tectonophysics*, 126, 99–124.